Energies **2015**, *8*, 5973-5996; doi:10.3390/en8065973

OPEN ACCESS

energies

ISSN 1996-1073

www.mdpi.com/journal/energies

Article

Evaluation of a Blade Force Measurement System for a Vertical Axis Wind Turbine Using Load Cells

Morgan Rossander *, Eduard Dyachuk, Senad Apelfröjd, Kristian Trolin, Anders Goude, Hans Bernhoff and Sandra Eriksson

Division of Electricity, Department of Engineering Sciences, Uppsala University, Box 534, 751-21 Uppsala, Sweden; E-Mails: eduard.dyachuk@angstrom.uu.se (E.D.); senad.apelfrojd@angstrom.uu.se (S.A.); k.trolin@gmail.com (K.T.); anders.goude@angstrom.uu.se (A.G.); hans.bernhoff@angstrom.uu.se (H.B.); sandra.eriksson@angstrom.uu.se (S.E.)

* Author to whom correspondence should be addressed; E-Mail: morgan.rossander@angstrom.uu.se; Tel.: +46-18-471-72-85.

Academic Editor: Frede Blaabjerg

Received: 24 March 2015 / Accepted: 5 June 2015 / Published: 18 June 2015

Abstract: Unique blade force measurements on an open site straight-bladed vertical axis wind turbine have been performed. This paper presents a method for measuring the tangential and normal forces on a 12-kW vertical axis wind turbine prototype with a three-bladed H-rotor. Four single-axis load cells were installed in-between the hub and the support arms on one of the blades. The experimental setup, the measurement principle, together with the necessary control and measurement system are described. The maximum errors of the forces and accompanying weather data that can be obtained with the system are carefully estimated. Measured forces from the four load cells are presented, as well as the normal and tangential forces derived from them and a comparison with theoretical data. The measured torque and bending moment are also provided. The influence of the load cells on the turbine dynamics has also been evaluated. For the aerodynamic normal force, the system provides periodic data in agreement with simulations. Unexpected mechanical oscillations are present in the tangential force, introduced by the turbine dynamics. The measurement errors are of an acceptable size and often depend on the measured variable. Equations are presented for the calculation of measurement errors.

Keywords: vertical axis wind turbine; blade force; measurement; wind power; tangential force; normal force; H-rotor

1. Introduction

The vertical axis wind turbine (VAWT) research at the Division of Electricity at Uppsala University has been going on for more than ten years. VAWTs are omnidirectional, and therefore, the yaw mechanism is excluded. Additionally, the generator may be placed at ground level. Major challenges associated with the design of VAWTs are the varying forces on the turbine and drive train [1]. To perform accurate scale experiments for wind turbines, the Reynolds number should match. For small-scale experiments (wind tunnels and water towing tanks), it is hard to reach realistic flows, as the Reynolds number is too low to obtain turbulent boundary layers. Therefore, it is important to carry out experiments at a larger scale to reach force coefficients similar to those of full-scale VAWTs.

Sandia National Laboratories conducted studies on force measurements of large-scale VAWTs with curved blades (Darrieus turbines) in the 1980s [2–4]. These experiments provided data with a high Reynolds number and are still used for the validation of simulation models of VAWTs [5–8]. However, data from force measurements on straight-bladed VAWTs (H-rotor) at high Reynolds numbers are still limited, since these require an operating VAWT at an open site. This motivates the type of measurement described in this work.

The 12-kW H-rotor built by Uppsala University in 2006 is a small-scale prototype designed for experimental purposes. The design has fixed blades, and the power absorption is controlled by adjusting the rotational speed though the control of the power output. This type of turbine is not reliably self-starting; instead, the generator is used as a motor to start the turbine. The starting process consumes negligible power and is described in [9]. The development and construction of the turbine prototype is further described in [10–12]. The generator is a directly-driven permanent magnet synchronous generator (PMSG) placed on the ground, designed to handle the varying power and rotational speed of the turbine [13]. The power coefficient of the turbine was studied in [14] and was found to peak at a value of 0.29 with a tip speed ratio of 3.3.

This paper evaluates a system for measuring the blade forces on the 12-kW VAWT by the use of four load cells attached between the support arms and the hub. Additionally, the control and measurement system for this experiment is described. The details, method, experimental setup and error estimations are described in Section 3. Example results and a discussion of the experimental approach are presented in Section 4. The conclusions are summarized in Section 5. First, Section 2 presents the underlying theory behind the studied forces.

2. Theory

2.1. Aerodynamic Blade Forces

The forces acting on the blade of a VAWT are shown in Figure 1. The wind speed at the blade $\vec{U}$ is usually lower in magnitude than the asymptotic wind speed $\vec{U}_\infty$, since the turbine extracts energy from the wind. The speed of the blade during rotation is:

$$\vec{U}_b = \Omega_{tur} R \hat{t} \tag{1}$$

where Ω_{tur} is the rotor angular velocity, R is the rotor radius and $\hat{t}$ is the unit vector in the tangential direction. The flow at the blade, due to its motion, is $-\vec{U}_b$, and the total flow velocity at the blade is $\vec{U}_{rel} = \vec{U} - \vec{U}_b$; see Figure 1. The angle of attack α is the angle between the chord line and the $\vec{U}_{rel}$, and the blade pitch angle δ is the angle between $\vec{U}_b$ and the chord line. The angle between $\vec{U}_{rel}$ and $\vec{U}_b$ is referred to as the angle of the relative wind, $\varphi = \alpha + \delta$. The lift force F_L is orthogonal to the relative wind vector $\vec{U}_{rel}$, and the drag force F_D is aligned with $\vec{U}_{rel}$. The tip speed ratio $\lambda = \frac{\Omega_{tur} R}{\vec{U}_\infty}$ influences the magnitude of the variation of α, which, in turn, affects the lift and drag force.

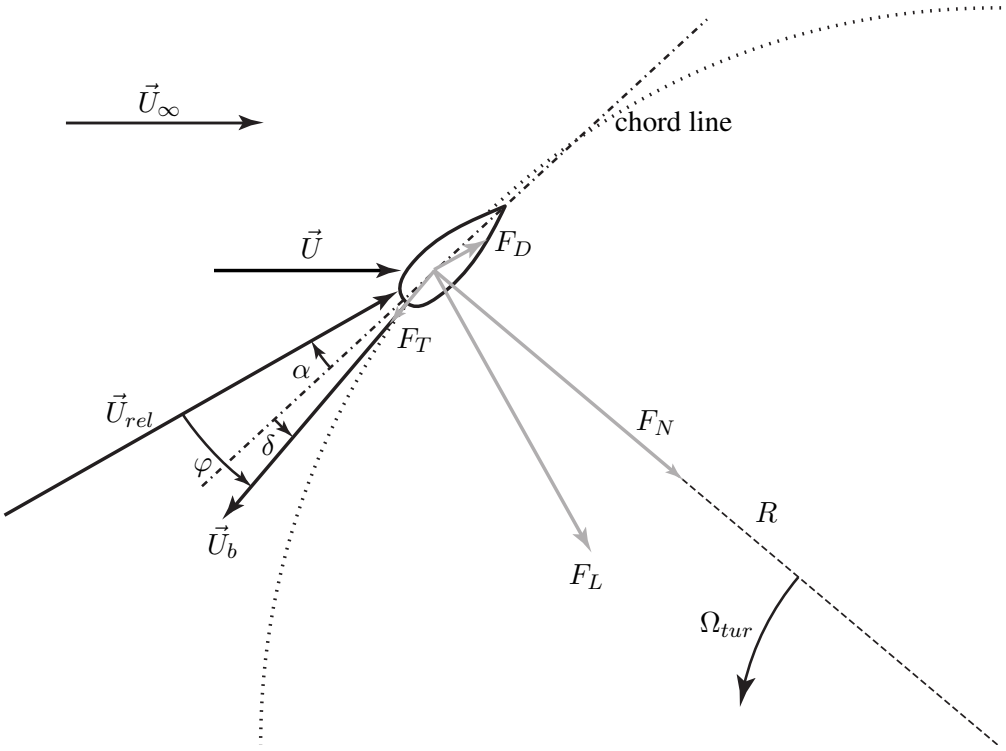

Figure 1. Notation of the velocities and forces acting on the blade of a VAWT. Note that in this paper, the positive direction of F_N will be outwards.

The resultant of F_L and F_D in the direction of the blade motion is denoted as the tangential force F_T, and the resultant of F_L and F_D in the radial direction is referred to as the normal force F_N. The tangential force F_T is used to estimate the turbine power, and the normal force F_N reflects the loads on the blades. The forces F_T and F_N are measured in this study according to the method described in Section 3.1.

2.2. Turbine Torque

The torque provided by one blade is:

$$\tau_B = F_T R \tag{2}$$

For constant wind speed, constant wind direction, non-turbulent wind and for a complete number of turbine revolutions, the average turbine torque can be expressed as:

$$\tau_{tur} = n_B \langle \tau_B \rangle_{rev} \tag{3}$$

where n_B is the number of blades and $\langle \tau_B \rangle_{rev}$ is the average torque provided by one blade for a complete number of revolutions.

2.3. Aerodynamic Simulation Model

The double multiple streamtube model is used in this study to obtain theoretical values of F_N and F_T. The model is based on the conservation of momentum, and it is described and tested in [8]. The only difference to the implementation in [8] is the dynamic stall modeling for low magnitudes of α. For an angle of attack α lower than half of the static stall angle α_{ss} (*i.e.*, for $|\alpha| < 0.5\alpha_{ss}$), the dynamic tangential force coefficient $C_{T,dyn}$ is substituted with the static $C_{T,st}$, found in [15]. For $0.5\alpha_{ss} < |\alpha| < \alpha_{ss}$, the linear scaling from $C_{T,st}$ to $C_{T,dyn}$ is applied to ensure the smooth transition between the static and the dynamic value of C_T. This modification is applied to ensure that the tangential coefficient approaches static values for low angles of attack.

3. Method

3.1. Blade Forces

Four sensors are used to measure the forces on one blade of the turbine. These are single-axis load cells, which measure tension and compression. The two blades without load cells were fitted with spacers of equal weight and radial dimension as the load cell assembly. Figures 2 and 3 show the assembly together with dimensions, the measured forces and the spacers for the unmeasured blades. To minimize the bending moment on the sensors, nuts were installed at both ends of each load cell, as seen in Figure 3. The sum of the measured forces F_0, F_1, F_2 and F_3 represents the radial force, F_R. Assuming that the rotational speed is constant, the radial force is the sum of the centrifugal force and the normal force, F_N, acting on the blade and support arms. Additionally, the differences between F_0, F_1 and F_2, F_3 is related to the tangential force, F_T, acting on the blade and support arms. Furthermore, the placement of the load cells allows for estimation of the bending moment of the blade and support arms, τ_{bend}. All of the forces and the bending moment can be summarized as:

$$F_R = F_0 + F_1 + F_2 + F_3 - F_{N,zero} \tag{4}$$

$$F_N = F_R - mL_C\Omega_{tur}^2 \tag{5}$$

$$F_T = \frac{L_1}{2L_B}\left(F_0 + F_2 - F_1 - F_3 - F_{T,zero}\right) \equiv \frac{L_1}{2L_B}F_{T,LC} \tag{6}$$

$$\tau_{bend} = \frac{L_0}{2}\left(F_0 + F_1 - F_2 - F_3 - F_{B,zero}\right) \equiv \frac{L_0}{2} F_{B,LC} \tag{7}$$

where $F_{T,LC}$ and $F_{B,LC}$ are introduced to simplify subsequent equations. The definition and values of the constant parameters (m, L_C, L_1, L_B, R) together with their estimated maximum errors are given in Table 1 and Figures 2 and 3. The weight of the structure and the tension in the assembly add offsets to the measured forces F_0, F_1, F_2 and F_3. The offsets can be identified as the no-load forces or zero values of the turbine. These zero values, $F_{N,zero}$, $F_{T,zero}$ and $F_{B,zero}$, are determined by:

$$F_{N,zero} = F_{0,zero} + F_{1,zero} + F_{2,zero} + F_{3,zero} \tag{8}$$

$$F_{T,zero} = F_{0,zero} + F_{2,zero} - F_{1,zero} - F_{3,zero} \tag{9}$$

$$F_{B,zero} = F_{0,zero} + F_{1,zero} - F_{2,zero} - F_{3,zero} \tag{10}$$

where $F_{0,zero}$, $F_{1,zero}$, $F_{2,zero}$ and $F_{3,zero}$ are the no-load forces measured by the load cells.

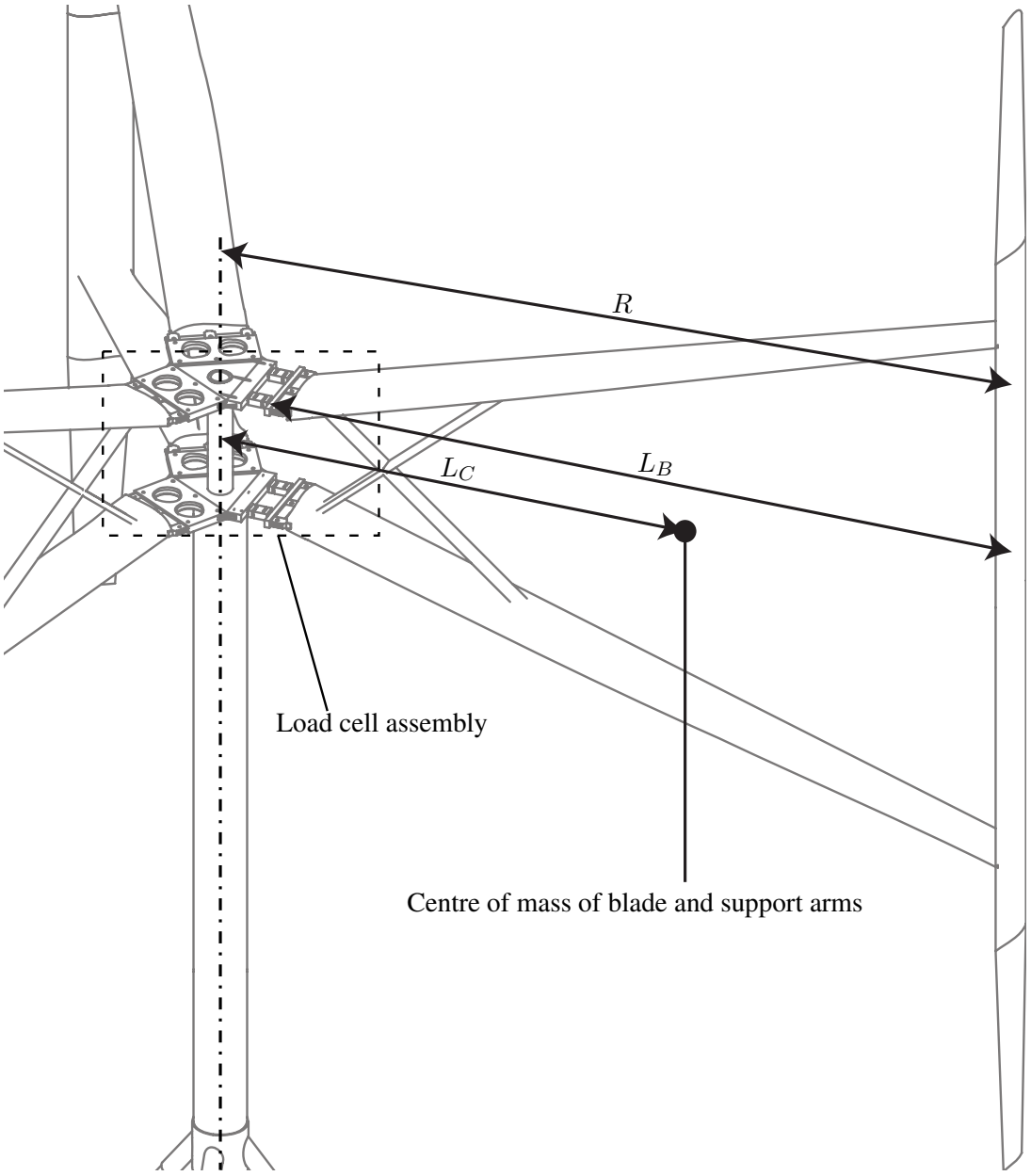

Figure 2. Load cell setup on the turbine.

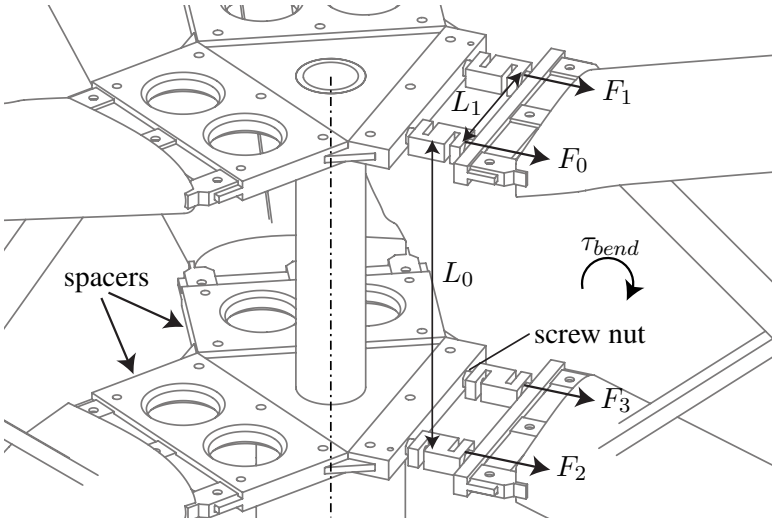

Figure 3. Length and force notations of the load cell assembly. Note that τ_{bend} is defined as bending around the tangential unit vector $\hat{t}$.

Table 1. Turbine parameters and estimated maximum error.

Measured Parameter	Value	Maximum Error
Turbine radius, R	3.24 m	±0.01 m
Center of mass, L_C	1.83 m	±0.01 m
Distance sensor to blade, L_B	2.99 m	±0.01 m
Vertical distance between sensors, L_0	0.500 m	±0.005 m
Horizontal distance between sensors, L_1	0.200 m	±0.0005 m
Mass of blade and support arms, m	35.79 kg	±0.05 kg
Turbine speed, Ω_{tur}		±0.05 rpm

The output of the sensors is measured by a National Instruments (NI) NI 9237 module, which interfaces directly with the load cells. The NI 9237 is mounted to a NI 9191 cDAQ WiFi chassis to transfer the signals to the control and data acquisition system (described in Section 3.6). Data are sampled at 2 kHz. The setup requires about 10 W of electric power, which is supplied through weather-protected brushes from the turbine tower. There is also a small buffer composed of batteries and capacitors connected to the power terminals inside the signal conditioning box.

The NI 9237 was calibrated together with the load cells. During the calibration procedure, each load cell was subjected to known tension and compression from weights. For each sensor, a linear curve fit was made of the calibration values. For all measurement values in this work, the curve fits are used to determine F_0, F_1, F_2 and F_3.

As a verification of the system, the support arms and the load cells were assembled and mounted on a wall in the laboratory. Known forces were applied at the center of the blade to imitate tangential and normal forces. The method of obtaining F_R according to Equation (4) was verified with deviations of less than 5 N for forces of 15 N to 140 N. The measurement of F_T according to Equation (6) was verified with deviations of less than ±3 N for tangential forces of 25 N to 105 N. Additionally, attempts were made to use the load cells to verify the position of the center of mass. This was unsuccessful,

since the no-load forces caused by tension in the assembly were difficult to separate from the mass of the assembly.

3.2. Load Cells

The load cells are sealed single-axis 4-wire cells with a capacity of ± 5000 N. The maximum capacity of the load cells was chosen to give good resolution at moderate wind speeds. Therefore, the load cells were intentionally chosen too weak to be used at the rated wind speed, as this wind speed is relatively uncommon at the site. It was considered preferable to have high accuracy at the more common wind speeds. The horizontal distance between the load cells was chosen as relatively low, as the radial forces are much stronger than the tangential forces. A short distance is required to get a sufficient difference in forces between the load cells to be able to calculate the torque. Hence, the distance was chosen to get a difference in forces that has a similar magnitude as the mean force.

3.3. Turbine

The turbine is a straight-bladed Darrieus turbine, also known as an H-rotor. There are two support arms for each blade, and the construction is reinforced by an interconnecting cross; see Figure 4. For this experiment, the original design of the turbine was modified to hold the load cells. The turbine radius has been increased and, therefore, also the swept area. The turbine power and rotational speed are limited with installed load cells, due to the capacity of the load cells, as described in Section 3.2. The turbine specifications are listed in Table 2.

Figure 4. The 12-kW turbine with installed load cells and spacers.

Table 2. The turbine characteristics.

Characteristic	Original	With Load Cells
Power	12 kW	
Rotational speed	127 rpm	
Rated blade tip speed	40 m/s	
Rated wind speed	12 m/s	
Number of blades	3	
Hub height	6 m	
Swept area	30 m^2	32 m^2
Turbine radius, R	3 m	3.2 m
Blade length	5 m	
Blade airfoil	NACA0021	
Chord length	0.25 m	
Tapering, linear	1 m (from tip)	
Tip chord length	0.15 m	
Blade pitch, δ	2°	2°

3.4. Generator and Shaft

The permanent magnet generator is located at the ground level and is directly connected to the turbine via a stiff shaft and a coupling, *i.e.*, there is no gearbox. The speed of the generator was measured using three Hall sensors mounted in the air gap of the generator. The sensors register the passing of the magnets. The speed was estimated from the switching times of these sensors. Due to imperfections in the geometry of the rotor, the estimation of the rotational speed can acquire some errors. To even out these variations during the rotation, a moving average of the speed estimations from ten electric periods ($\frac{10}{16}$ of one revolution) was used as the current speed value. For fixed speed operation and for a complete number of revolutions, these errors will cancel out. Therefore, the total error of the speed estimation is assumed to be low, as seen in Table 1.

3.5. Weather and Site Conditions

The location of the turbine is the Marsta Meteorological Observatory ($59°55'32''$ N, $17°35'12''$ E) close to Uppsala, Sweden. The site has well-known weather conditions and a convenient location, rather than the potential of high wind energy production [16]. The turbine is positioned fairly close to the ground and to some obstacles that cause turbulence. Therefore, good knowledge of the wind direction will make it possible to choose data when the wind is less affected by the obstacles. The wind speed, wind direction, air temperature, air pressure and air humidity were measured with a Vaisala WXT520. The WXT520 is placed 15 m north of the turbine at hub height. The position is chosen to limit the disturbances from the turbine from the dominating wind direction, which also is the direction of lowest turbulence due to the site obstacles. The distance, 15 m or 2.5 turbine diameters, is based on

the recommendations in [17]. The WXT520 has a serial digital RS-485 output protocol, which limits all of the weather measurement errors to the WXT520 device. All weather data were sampled at 1 Hz.

The wind speed and air density are important for the interpretation of the collected forces. The air density can be determined as:

$$\rho = \frac{1}{T}\left(\frac{p}{287.1} - 2.700 \cdot 10^{-10} h \exp\left(0.06318(T + 273.15)\right)\right) \tag{11}$$

where p is the air pressure in Pa, h is the relative humidity in percent (%RH) and T is the temperature in °C [17]. The maximum error of ρ can be estimated in the same manner as described in Section 3.8. All maximum errors from weather measurements are specified in Table 3.

Table 3. Maximum error of the weather measurements.

Measured Parameter	Max Error		Comments
Wind speed	$\Delta U_\infty =$	±0.3 m/s	at 0 m/s to 10 m/s
		±3 %	at 10 m/s to 35 m/s
Wind direction	$\Delta W_{dir} =$	±3.0°	
Barometric pressure	$\Delta p =$	±0.05 Pa	at 0 °C to 30 °C
		±0.1 Pa	at −52 °C to 60 °C
Air temperature	$\Delta T =$	±0.3 °C	
Air humidity	$\Delta h =$	±3 %RH	at 0 %RH to 90 %RH
		±5 %RH	at 90 %RH to 100 %RH
Air density	$\Delta \rho =$	±0.0016 kg/m^3	calculated from Δp, ΔT, Δh
			valid for $T < 15$ °C, $h < 90$ %RH

3.6. Control and Data Acquisition

The control and logging software was developed in National Instruments LabVIEW. A total of three executables were running simultaneously, one on each platform; FPGA, real-time target (RT) and Windows Server 2008. A simplified illustration of the data and power flow can be seen in Figure 5. The AC output from the generator varies in frequency, and the voltage is diode-rectified into a DC-voltage. The DC-voltage is fed into a two-level (2L) inverter. To regulate the turbine speed, a PI-controller was implemented on the FPGA. The turbine speed was used as input and the modulation level of the inverter as output. The controller loop speed was 10 Hz, and a conditional anti-windup was used. The conditional anti-windup provides acceptable performance without adding more parameters to the controller [18]. The controller parameters were found from a simulation of the turbine and then fine-tuned by tests on site.

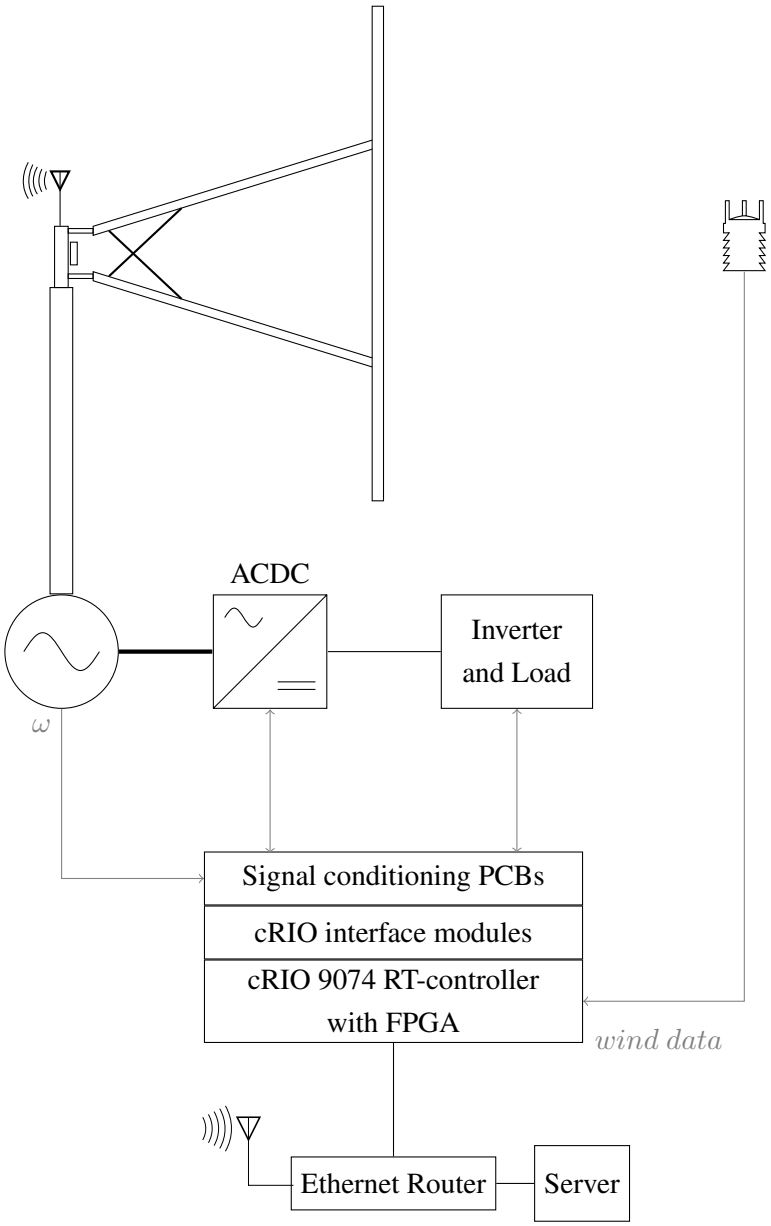

Figure 5. Overview of the control and measurement system.

The power, rotational speed, controller output and weather conditions were sampled by the FPGA, transferred to the RT-controller and then transferred to the server for calibration and synchronization with the forces F_0, F_1, F_2 and F_3. All data were stored on the server hard drive. The system has additional components for start, safety and control that are outside the scope of this paper.

3.7. Blade Position

The position θ of the blade (often referred to as the "azimuth angle") is calculated through the response of the normal force F_N. The normal force on the blade is close to zero when the blade passes from upwind to the downwind side of the rotor; see Figure 6. It is assumed that during constant rotational speed, the blade is at $\theta = 90^\circ$ when passing the middle of the upwind disk during one revolution; Figure 6. The start position of the blade θ is updated on every revolution.

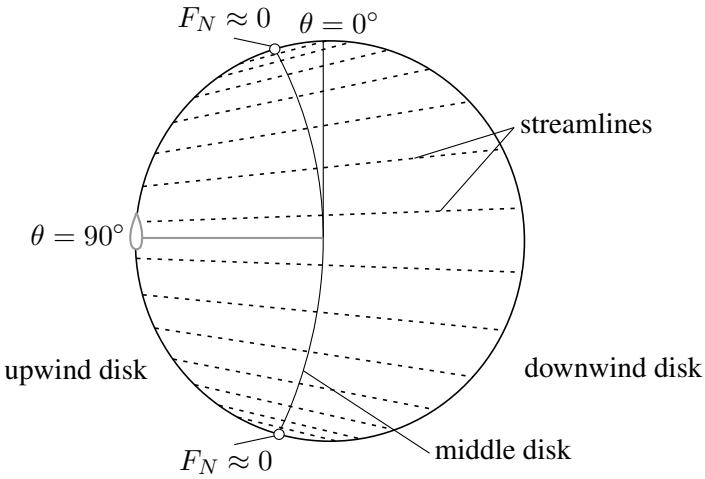

Figure 6. Definition of the blade azimuth angle θ from the normal force.

3.8. Error Estimation Method

The error of a value Z derived from measured values x, y, ... can be determined by the mean error:

$$\langle \Delta Z \rangle = \sqrt{\left(\frac{\partial Z}{\partial x}\right)^2 (\Delta x)^2 + \left(\frac{\partial Z}{\partial y}\right)^2 (\Delta y)^2 + \dots} \tag{12}$$

or the maximum error:

$$|\Delta Z| = \left|\frac{\partial Z}{\partial x}\Delta x\right| + \left|\frac{\partial Z}{\partial y}\Delta y\right| + \dots \tag{13}$$

where Δx and Δy are the maximum errors of the measured values. The mean error estimation method is only valid if all contributing errors can be considered independent of each other. As can be seen by Equations (3) to (7), the F_R, F_N, F_T and τ_{bend} depend on several different measurements. The errors of some of the measurements have some correlation. To handle such partly correlated measurements, the method of maximum error was chosen; Equation (13). This approach gives a large error span, and it is important to note that all errors given in this paper are maximum errors, unless otherwise stated.

For the turbine parameters, maximum errors were estimated based on the tools and the measurement technique; see Table 1. The maximum errors for the individual load cells ΔF_0, ΔF_1, ΔF_2 and ΔF_3 were estimated as the sum of the maximum deviation from the linear calibration curve (see Section 3.1), the maximum error of the weight measurement (for calibration) and the highest error in the load cell specification.

The no-load zero values $F_{N,zero}$, $F_{T,zero}$ and $F_{B,zero}$ had to be found as an average during low wind speeds, since aerodynamic forces on the turbine were always present just before a measurement. To estimate the zero values, the load cell output values were grouped in 200 s periods when the wind speed was below 1 m/s. The averages of those periods were used to get a baseline of the deviation in the zero values over time. The most deviating temperatures (>15 °C) were discarded from the zero value estimations. The remaining data resulted in 1300 datasets of F_0, F_1, F_2 and F_3. The zero values $F_{N,zero}$, $F_{T,zero}$ and $F_{B,zero}$, which all vary with time and temperature, were calculated for each set. The maximum errors, $\Delta F_{N,zero}$, $\Delta F_{T,zero}$ and $\Delta F_{B,zero}$ were taken as the maximum deviation found

in all of the sets. Any additional errors in the load cell measurements caused by temperature or the measurement electronics were assumed to be included in ΔF_0, ΔF_1, ΔF_2, ΔF_3, $\Delta F_{N,zero}$, $\Delta F_{T,zero}$ and $\Delta F_{B,zero}$.

Finally, the estimated maximum errors are determined by applying Equation (13) on Equations (3) to (7). Equations (16) and (17) can be simplified to depend on the actual measured value,

$$\Delta F_R = |\Delta F_0| + |\Delta F_1| + |\Delta F_2| + |\Delta F_3| + |\Delta F_{N,zero}| \tag{14}$$

$$\Delta F_N = |\Delta F_R| + |L_C \Omega_{tur}^2 \Delta m| + |m \Omega_{tur}^2 \Delta L_C| + |2 \Omega_{tur} m L_C \Delta \Omega_{tur}| \tag{15}$$

$$\Delta F_T = \frac{L_1}{2L_B} \left(|\Delta F_0| + |\Delta F_1| + |\Delta F_2| + |\Delta F_3| + |\Delta F_{T,zero}| + \left| \frac{F_{T,LC}}{L_1} \Delta L_1 \right| + \left| \frac{F_{T,LC}}{L_B} \Delta L_B \right| \right) \tag{16}$$

$$\Delta \tau_{bend} = \frac{L_0}{2} \left(|\Delta F_0| + |\Delta F_1| + |\Delta F_2| + |\Delta F_3| + |\Delta F_{B,zero}| \right) + \left| \frac{F_{B,LC}}{2} \Delta L_0 \right| \tag{17}$$

$$\Delta \tau_{tur} = n_B \left(\langle |F_T \Delta R| \rangle + |R \Delta F_T| \right) \tag{18}$$

3.9. Experimental Procedure

The measurement campaign was from 13 September to 4 December 2014. For baseline purposes (see Section 3.8), the load cell data was being sampled at a large portion of that time with the turbine off. Actual running field tests were limited to times of suitable conditions. The weather conditions during the measurements divided the data into steady and turbulent conditions.

During the field tests, the speed controller was manually set to a speed that corresponded to reasonable power extraction from the turbine based on actual wind conditions. Since conditions at the site varied and the rotational speed was kept constant for some time, the resulting datasets had a wide spread in tip speed ratios. Data at different tip speed ratios are valuable for comparison with models.

4. Results and Discussion

4.1. Influence of Load Cells on the Turbine Dynamics

As described in Section 3.1, the load cell assembly on Blade 1 alters the dynamics of the turbine. The spacers used on Blades 2 and 3 are assumed to be fairly stiff, and the properties of Blades 2 and 3 should be similar to the original turbine design (with the modified radius). To evaluate the extent of the change on Blade 1, the natural frequencies of all of the blades were analyzed using an accelerometer. The test was carried out on site on the fully-assembled modified turbine. The accelerometer was temporarily attached to each blade at 400 mm from the lower end. The turbine was excited by impulse forces. The blades were tested one by one. During measurement of Blade 1, the load cells were activated to validate the accelerometer measurements and to confirm the mode shapes. The measurement discovered that the blades had the same set of modes for frequencies below 40 Hz.

The measured frequencies for the blades are presented in Table 4. How the different modes were excited is listed in the table and illustrated in Figure 7. The bending modes have the same frequency for all blades. The twisting frequency of Blade 1 has dropped by 16 % compared to Blade 2 and 23 %

compared to Blade 3. The tangential mode at 8.0 Hz of Blade 1 represents a 12 % drop compared to Blades 2 and 3.

The normal modes are the same for Blades 1 and 2, and there is a small difference for Blade 3. A possible explanation is that Blades 1 and 2 are reinforced with fiberglass, while Blade 3 has carbon fiber reinforcements. The weights are the same, but the stiffness properties are different. The two natural frequencies in the normal direction were only present in the accelerometer spectrum. The frequencies are therefore assumed to represent the natural frequencies of the blade in the normal direction. This is supported by the difference in frequency for Blade 3 in the normal modes. The absence of other natural frequencies in normal mode indicates that the support arms are very stiff in the normal direction.

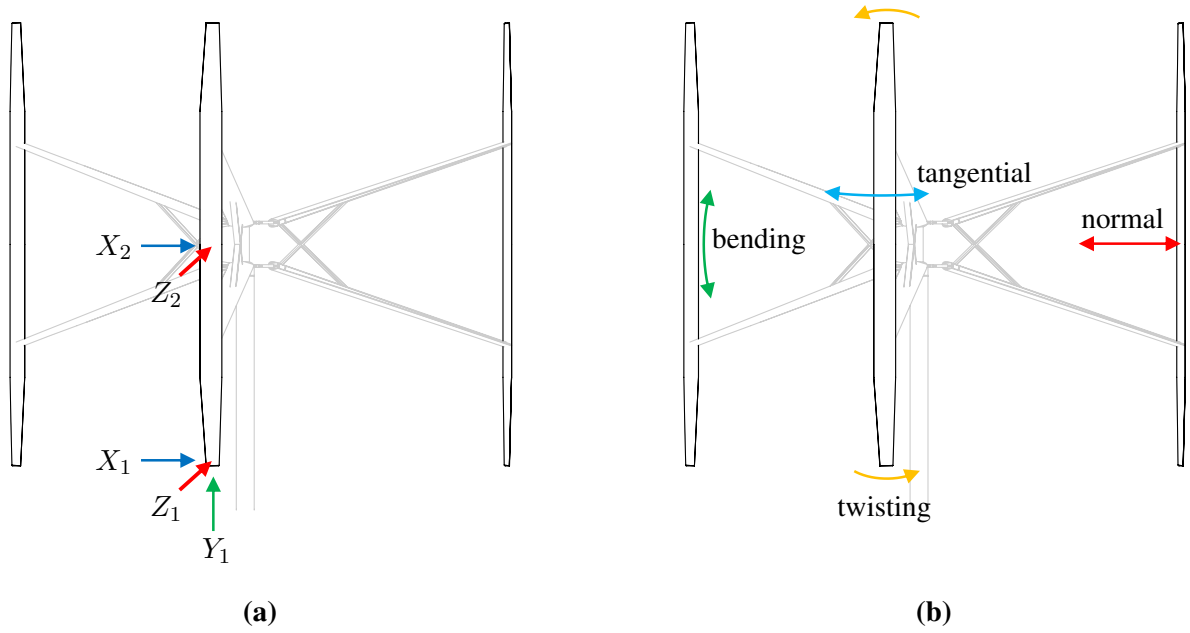

Figure 7. Turbine natural frequencies: (**a**) excitation; (**b**) modes of modes of movement.

Table 4. Measured natural frequencies of the blade assemblies. The excitations and modes are illustrated in Figure 7.

Mode	Blade 1 [1] (Hz)	Blade 2 (Hz)	Blade 3 [2] (Hz)	Excitation
Twisting	5.6	6.7	7.3	X_1
Tangential 1	8.0	9.1	9.1	X_2
Tangential 2 [3]	28.8	29.6	36.1	X_2
Bending 1	3.2	3.2	3.2	Y_1
Bending 2	4.6	4.6	4.6	X_1
Normal 1 [4]	13.5	13.2	12.6	Z_2
Normal 2 [4]	20.7	20.7	18.7	Z_1

Notes: [1] Blade with the load cells; [2] Blade reinforced with carbon fibre; [3] Clear in accelerometer spectrum, weak in load cell spectrum; [4] Only visible in accelerometer spectrum.

The lowered natural frequency in tangential mode indicates that the load cell blade assembly is a softer system in the tangential direction than the other blades. Since the dynamics in the bending direction (up and down) is unchanged, the lowered twisting mode frequency is presumably also a result of the increased softness in the tangential direction. For the tangential mode around 30 Hz, the spectral amplitude was high in the accelerometer data, but hardly visible in the load cell spectrum. This frequency is therefore assumed to be the natural frequency of the blade in the tangential direction. This is also supported by the higher frequency of Blade 3 for this mode.

4.2. Accuracy

The resulting maximum errors of the calibrations and zero values are listed in Table 5. The accuracy of the data that can be obtained is an important result of the presented method. The maximum errors based on the parameters in Table 1, the measurements in Table 5 and Equations (14) to (18) give the resultant maximum measurement errors as:

$$\Delta F_R = \pm 23\,\text{N} \tag{19}$$

$$\Delta F_N = \pm(0.0049\Omega_{tur,rpm}^2 + 0.072\Omega_{tur,rpm} + 23)\ [\text{N}] \tag{20}$$

$$\Delta F_T = \pm(0.0058|F_T| + 1.1)\ [\text{N}] \tag{21}$$

$$\Delta \tau_{bend} = \pm(0.010|\tau_{bend}| + 20)\ [\text{Nm}] \tag{22}$$

$$\Delta \tau_{tur} = \pm(0.087\langle|F_T|\rangle + 11)\ [\text{Nm}] \tag{23}$$

As was explained in Section 3.8, the maximum error was considered to be the most suitable method for the measurements. For comparison, the mean error has been calculated according to Equation (12), and it is about half of the maximum errors given in Equations (19) and (23).

The radial force has a constant maximum error $\Delta F_R = \pm 23\,\text{N}$, of which the calibration error contributes to $\pm 12\,\text{N}$, the no-load error to load $\pm 7\,\text{N}$ and the load cell hysteresis $\pm 4\,\text{N}$; see Table 5. For the maximum error of the normal force, two more terms are added because of the centrifugal force. In the span 40 rpm to 90 rpm, the maximum error goes from $\pm 34\,\text{N}$ to $\pm 70\,\text{N}$.

Table 5. Maximum errors of zero and calibration values.

Measured Parameter	Value	Maximum Error
$F_{N,zero}$	15 N	$\Delta F_{N,zero} = \pm 7\,\text{N}$
$F_{T,zero}$	37 N	$\Delta F_{T,zero} = \pm 18\,\text{N}$
$F_{B,zero}$	1960 N	$\Delta F_{B,zero} = \pm 63\,\text{N}$
F_0		$\Delta F_0 = \pm 2.2\,\text{N}$
F_1		$\Delta F_1 = \pm 5.9\,\text{N}$
F_2		$\Delta F_2 = \pm 4.2\,\text{N}$
F_3		$\Delta F_3 = \pm 4.1\,\text{N}$

The tangential force has a weak dependence on its own value. At $F_T = 100\,\text{N}$, the maximum error has only increased from $\pm 1.1\,\text{N}$ to $\pm 1.6\,\text{N}$. The maximum error of torque has slightly higher dependence

on F_T and peaks around $\pm 20\,\text{Nm}$ at $F_T = 100\,\text{N}$. The maximum error of the bending moment of the blade is fairly close to constant and may be approximated to $\Delta\tau_{bend} \approx \pm 25\,\text{Nm}$ with $|\tau_{bend}| < 500\,\text{Nm}$.

4.3. System Output and Performance

An example force measurement for three complete revolutions is captured in Figure 8. Wind speed and wind direction are fairly constant, and the system is keeping the rotational speed fixed. The output from the load cells appears very oscillatory. The resulting forces from the load cell data in Figure 8 are shown in Figure 9. It is revealed that the mechanical oscillations are limited to the tangential force and the bending moment, leaving the normal force with a remarkably smooth appearance. Tests to reveal the operational limits discovered that the speed limit was about $90\,\text{rpm}$ and the maximum power was about $4\,\text{kW}$. Additionally, during the measurement campaign, the weather conditions were a further limitation.

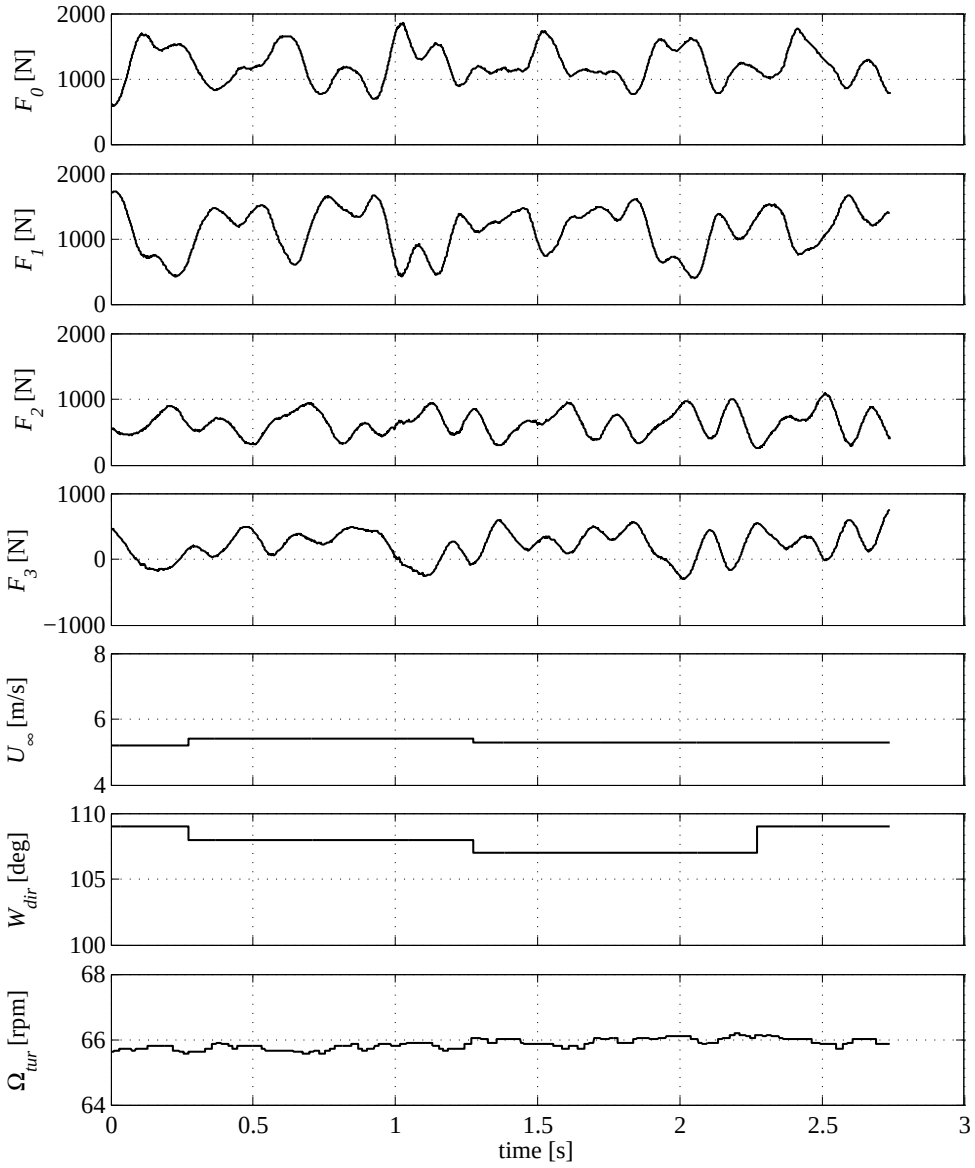

Figure 8. Load cells output, wind speed, wind direction and rotational speed during three turbine revolutions.

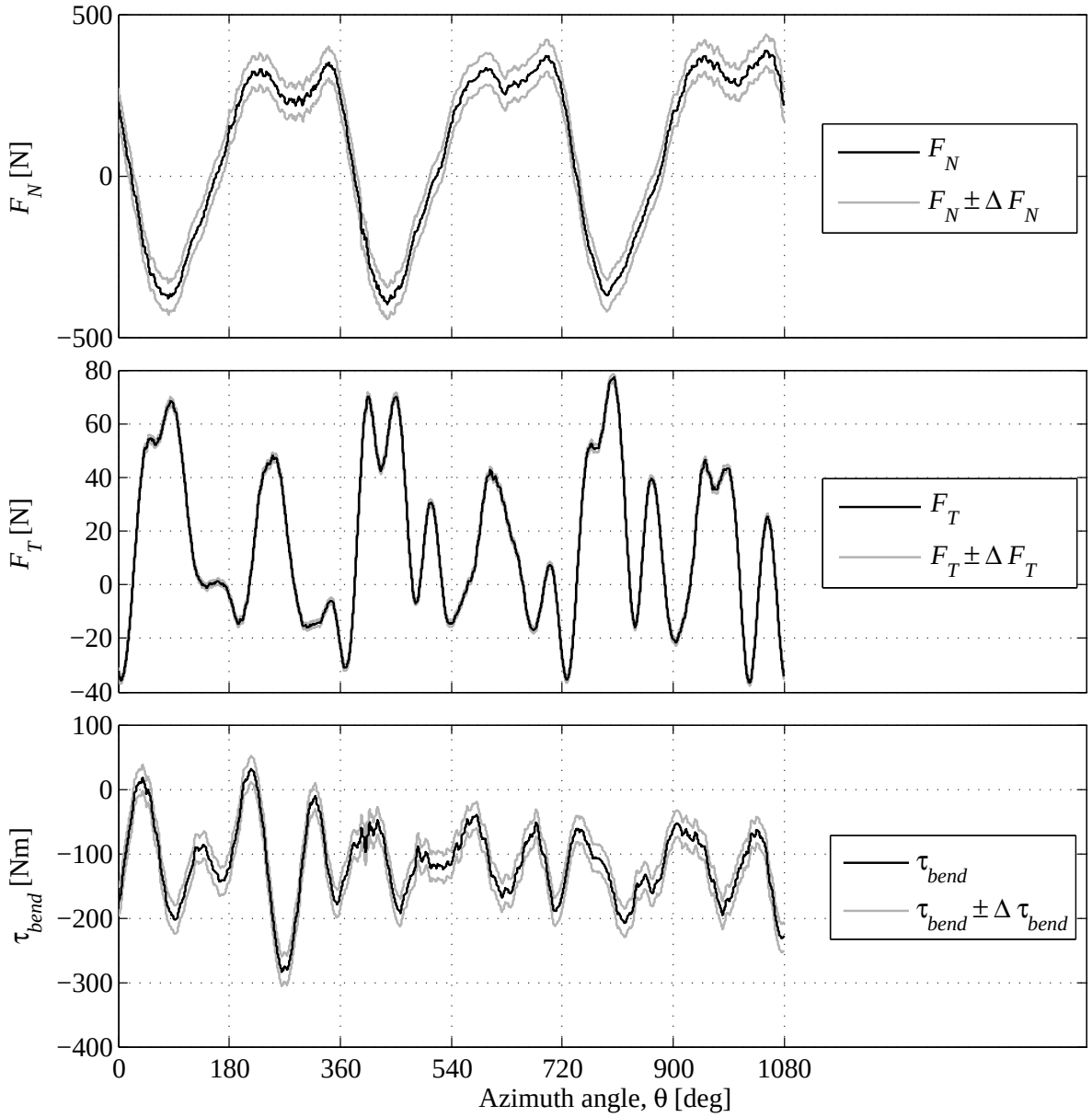

Figure 9. Estimations of F_N, F_T and τ_{bend} and the maximum error from the data in Figure 8. Tip speed ratio $\lambda = 4.31$, $\langle \Omega_{tur} \rangle = 65.73\,\mathrm{rpm}$, air density $\rho = 1.239\,\mathrm{kg/m^3}$.

4.4. Radial and Normal Force

To illustrate the performance of the proposed method in the normal direction, the measured normal force has been determined for two additional occasions. Figure 10 shows that the shape of the measured F_N is close to the expected F_N obtained from the simulation model (Section 2.3). The maximum magnitude of F_N increases with higher rotational speed at a constant tip speed ratio. This is due to the higher velocities at the blades and higher Reynolds number, and it agrees with the model prediction. The oscillations of the measured F_N at $180° < \theta < 360°$ are consistent and present during each revolution.

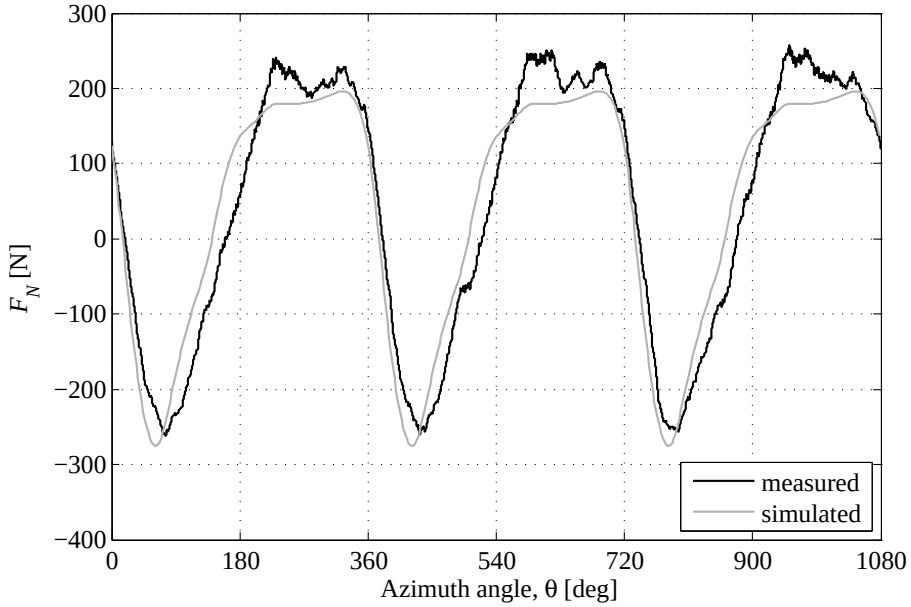

(a)

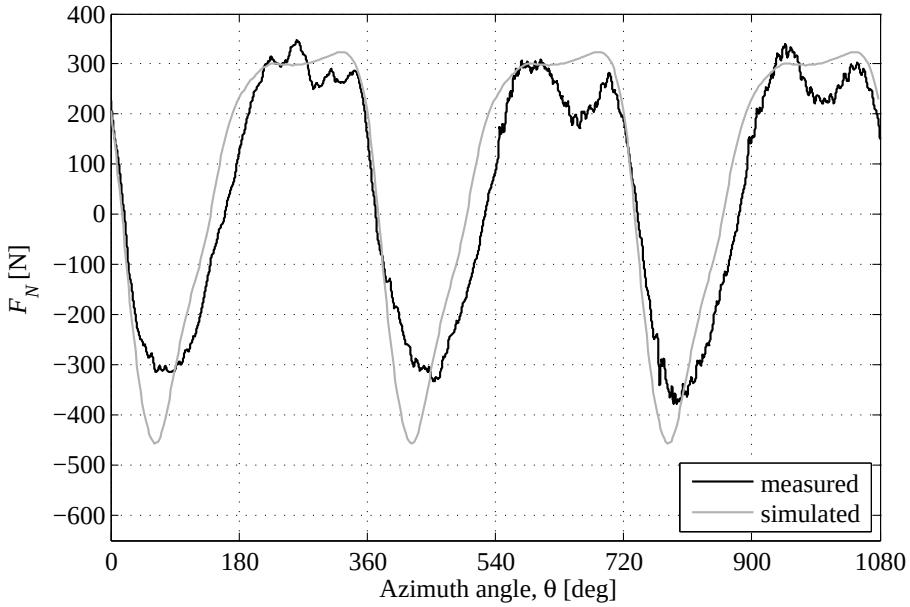

(b)

Figure 10. Comparison of measurements and simulations of F_N for two different rotational speeds. (**a**) Normal force response at $\lambda = 3.59$ and $\langle \Omega_{tur} \rangle = 50.63\,\mathrm{rpm}$. Air density $\rho = 1.275\,\mathrm{kg/m^3}$; (**b**) Normal force response at $\lambda = 3.58$ and $\langle \Omega_{tur} \rangle = 64.67\,\mathrm{rpm}$. Air density $\rho = 1.236\,\mathrm{kg/m^3}$.

The maximum error of the normal force in Figure 9 is $\Delta F_N = \pm 49\,\mathrm{N}$. Since the average of the rotational speed is used in determination of F_N, the only difference to F_R is actually a constant, depending on the rotational speed. Therefore, the maximum error of the shape of F_N is the same as the maximum error of F_R. That is a fair improvement, since $\Delta F_R = \pm 23\,\mathrm{N}$, which is less than half of ΔF_N.

4.5. Tangential Force and Torques

To further illustrate the behavior of the proposed method in the tangential direction, the measured tangential force has been determined for two additional occasions. The tangential force contains large oscillations of multiple frequencies; see Figures 9 and 11. These oscillations are dependent on the rotational speed and are not predicted by the model; see Figure 11. For almost identical tip speed ratios, the shape of F_T is different at different rotational speeds, which is contrary to the simulated values. In Figure 9, F_T has a span from -37 N to 77 N. The average value, which provides the actual torque, is only 15.6 N. As shown in Section 4.1, the load cells change the dynamics of the system. The indicated change is low, and therefore, the behavior seen may reflect the tangential forces on the other blade assemblies. Furthermore, it is important to note that the blade force is measured at the hub. Since the support arms may act as a damper, the force on the blade may be higher or lower. The other blades that are unmeasured are likely also to provide oscillating forces, which could affect the hub and the force sensors. Some of the mechanical oscillations seen may therefore actually be the result of all three blades. It should be noted that the operating power is quite low (< 10 % of the rated power) and that these mechanical oscillations are possibly less significant at higher operating power. Overall, the tangential force measurement can provide interesting data of the mechanical dynamics of the prototype, but limited knowledge of the aerodynamic tangential force acting on the blade. The mechanical oscillations require further analysis.

The maximum error of the tangential force presented in Figure 9 is $\Delta F_T = \pm 1.6$ N. That is good compared to the peak values. However, it is a larger fraction of the average F_T. Higher operational power would improve the relative size of the maximum error since ΔF_T is fairly constant; see Equation (21). As described in Section 4.3, the operational power is limited.

With all blades providing equal torque, the average torque in Figure 9 is 152 ± 13 Nm. The assumption that all blades provide equal torque is a possible source of more errors. By using the average of many complete revolutions, that assumption can be justified. For more accurate torque measurements, a rotational torque sensor is probably better or by estimation from the electric power output of the generator, as in [14].

The bending moment on the blade, τ_{bend}, also seems affected by oscillations; see Figures 9 and 12. The shape of τ_{bend} changes with different rotational speeds. Note that τ_{bend} is not calculated by the simulation model described in [8]. Due to the wind shear pushing the upper and lower part of the blade unequally, the value of τ_{bend} is expected to change from positive to negative during one revolution. The presented data, however, have a constant negative offset. The center of mass of the blade and support arms is shifted vertically because of the gravitational force. The centrifugal force acts on the shifted center of mass, causing the constant offset. The measured behavior should be representative for the movement of the other blades, since the dynamics of the measurement blade and that of the other blades are the same in the bending direction; see Section 4.1.

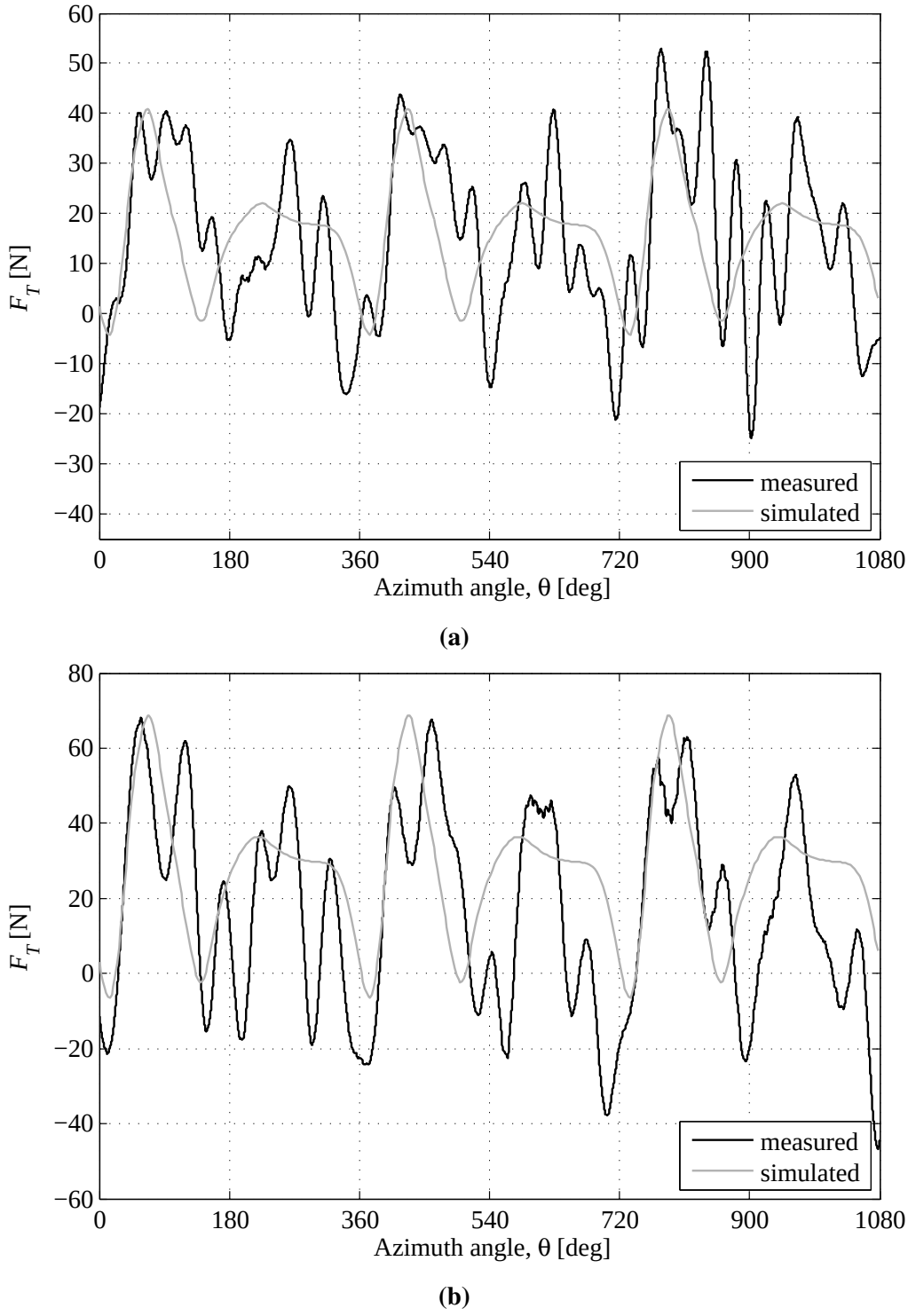

Figure 11. Comparison of measurements and simulations of F_T for two different rotational speeds. (**a**) Tangential force response at $\lambda = 3.59$ and $\langle \Omega_{tur} \rangle = 50.63\,\mathrm{rpm}$. Air density $\rho = 1.275\,\mathrm{kg/m^3}$; (**b**) Tangential force response at $\lambda = 3.58$ and $\langle \Omega_{tur} \rangle = 64.67\,\mathrm{rpm}$. Air density $\rho = 1.236\,\mathrm{kg/m^3}$.

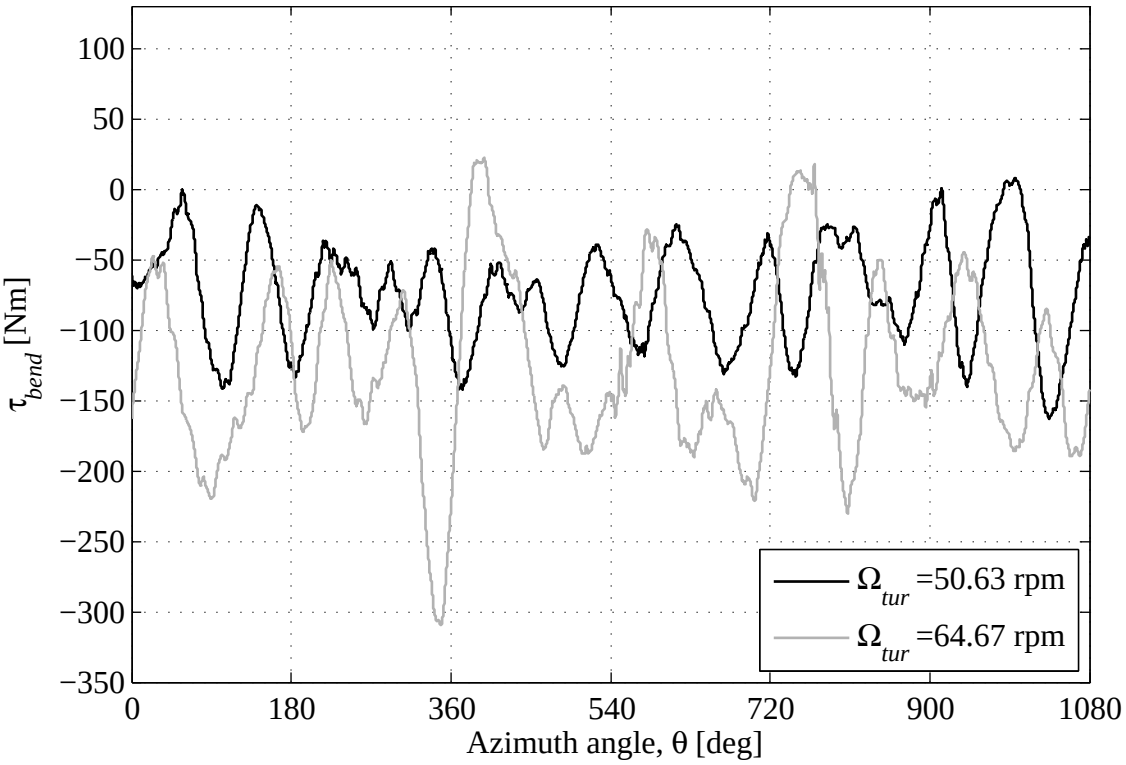

Figure 12. Comparison of the measured τ_{bend} for two different rotational speeds.

4.6. General Discussion

The accuracy of the load cells is fairly high compared to the other factors affecting the total accuracy of the measurement. The operating power could be increased with load cells of higher capacity, without significant loss in accuracy of the normal force. Additionally, the horizontal separation of the load cells can be wider to increase stability in the tangential direction, hopefully lowering the mechanical oscillations. However, this would decrease the tangential force accuracy. As has been shown, the presented method already has limitations on measuring the average tangential force with high accuracy, so that can be a fair trade off.

It can be realized that good steady conditions of a desirable nature can be rare for open site experiments. This means that the experimental setup must be operational and ready for long periods of time, waiting for perfect conditions. This is of course a large practical challenge with prototypes and measurement systems in open site experiments.

5. Conclusions

A method for analyzing the aerodynamic blade forces using load cells at the hub of a vertical axis wind turbine has been presented and experimentally evaluated. The method was intended for both tangential and normal blade force measurements. The method provides a normal force with good periodicity over turbine revolutions and good agreement with theoretical values.

For the tangential force, mechanical oscillations have been discovered. The peak amplitudes of the measured forces are of a similar size as in the simulations. The shape of the tangential force is clearly

distorted by the dynamics of the turbine. The presented method is therefore unsuited to estimation of the tangential aerodynamic forces acting on the blade. However, the provided data can still be interesting for studying the mechanical dynamics of the turbine. It should be noted that the turbine power during the tests was $5\,\%$ to $10\,\%$ of nominal.

The accuracy of the measurements of forces and accompanying weather conditions has been investigated carefully. Many of the errors are dependent on the measured values, and equations have been derived to simplify the estimations of the different errors. The measurements can be considered to be fairly accurate.

A final conclusion from this study is that open site experiments might be time-consuming, since they suffer from being dependent on the current weather conditions and, in this case, also require steady wind conditions.

Acknowledgments

The J. Gust Richert foundation is acknowledged for contributions for equipment for the load cell experiments. This work was conducted within the STandUp for Energy strategic research framework. Rickard Petterson is acknowledged for obtaining the geodata of the experimental site. The authors also want to thank Dana Salar for the help with modification of the turbine.

Author Contributions

Morgan Rossander has done the majority of the experimental work and written most of the paper. Morgan Rossander and Eduard Dyachuk have done the turbine modifications and load cell calibrations. Morgan Rossander, Eduard Dyachuk, Sandra Eriksson and Anders Goude have all taken part in data analysis and interpretation. Senad Apelfröjd, Kristian Trolin, Anders Goude and Hans Bernhoff have planned and designed the load cell setup and measurement system. Sandra Eriksson and Hans Bernhoff have supervised the project.

Conflicts of Interest

The authors declare no conflict of interest.

Nomenclature

Δ		Maximum error of parameter
α	deg	Angle of attack
δ	deg	Pitch angle
φ	deg	Angle of the relative wind
θ	deg	Azimuth angle
F_0	N	Load Cell 0 force
F_1	N	Load Cell 1 force
F_2	N	Load Cell 2 force
F_3	N	Load Cell 3 force

$F_{0,zero}$	N	Load Cell 0 no-load force
$F_{1,zero}$	N	Load Cell 1 no-load force
$F_{2,zero}$	N	Load Cell 2 no-load force
$F_{3,zero}$	N	Load Cell 3 no-load force
$F_{B,LC}$	N	Bending force load cell input, offset removed
$F_{B,zero}$	N	Bending force, zero value
F_D	N	Drag force
F_L	N	Lift force
F_N	N	Aerodynamic normal force
$F_{N,zero}$	N	Aerodynamic normal force, zero value
F_R	N	Radial force
F_T	N	Tangential force
$F_{T,LC}$	N	Tangential force load cell input, offset removed
$F_{T,zero}$	N	Tangential force, zero value
g	m/s^2	Local gravity
h	%RH	Air humidity
λ		Tip speed ratio (TSR)
L_0	m	Vertical distance between sensors
L_1	m	Horizontal distance between sensors
L_B	m	Distance sensors to blade
L_C	m	Distance load cells to center of mass
m	kg	Mass of blade and support arms
n_B		Number of blades
Ω_{tur}	rad/s	Turbine rotational speed
$\Omega_{tur,rpm}$	rpm	Turbine rotational speed (rpm)
p	Pa	Barometric pressure
R	m	Turbine radius
ρ	kg/m^3	Air density
T	°C	Air temperature
$\hat{t}$		Unit vector in tangential direction
τ_{bend}	Nm	Bending moment of the blade
τ_B	Nm	Blade torque
$\langle\tau_B\rangle_{rev}$	Nm	Blade torque, average over full revolutions
τ_{tur}	Nm	Turbine torque, average over full revolutions
$\vec{U}_\infty$	m/s	Wind speed
U_∞	m/s	Wind speed magnitude, $\lvert\vec{U}_\infty\rvert$
$\vec{U}_b$	m/s	Speed of blade
$\vec{U}$	m/s	Wind speed at blade
$\vec{U}_{rel}$	m/s	Relative wind
W_{dir}	deg	Wind direction

References

1. Sutherland, H.J.; Berg, D.E.; Ashwill, T.D. A retrospective of VAWT technology. In *Technical Report SAND2012-0304*; Sandia National Laboratories: Albuquerque, NM, USA, 2012.
2. Johnston, S.F. Proceedings of the Vertical Axis Wind Turbine (VAWT) Design Technology Seminar for Industry. In *Technical Report SAND80-0984*; Sandia National Laboratories: Albuquerque, NM, USA, 1980.
3. Akins, R.E. Measurements of Surface Pressures on an Operating Vertical-Axis Wind Turbine. In *Technical Report SAND89-7051*; Sandia National Laboratories: Albuquerque, NM, USA, 1989.
4. Oler, J.; Strickland, J.; Im, B.; Graham, G. Dynamic stall regulation of the Darrieus turbine. In *Technical Report SAND83-7029*; Sandia National Laboratories: Albuquerque, NM, USA, 1983.
5. Ahmadi-Baloutaki, M.; Carriveau, R.; Ting, D.S.K. Straight-bladed vertical axis wind turbine rotor design guide based on aerodynamic performance and loading analysis. *Proc. Inst. Mech. Eng. Part A J. Power Energy* **2014**, *228*, 742–759.
6. Ferrari, G. Development of an Aeroelastic Simulation for the Analysis of Vertical-Axis Wind Turbines. Ph.D. Thesis, The University of Auckland, Auckland, New Zealand, 2012.
7. Shires, A. Development and Evaluation of an Aerodynamic Model for a Novel Vertical Axis Wind Turbine Concept. *Energies* **2013**, *6*, 2501–2520.
8. Dyachuk, E.; Goude, A. Simulating Dynamic Stall Effects for Vertical Axis Wind Turbines Applying a Double Multiple Streamtube Model. *Energies* **2015**, *8*, 1353–1372.
9. Kjellin, J.; Bernhoff, H. Electrical starter system for an H-rotor type VAWT with PM-generator and auxiliary winding. *Wind Eng.* **2011**, *35*, 85–92.
10. Solum, A.; Deglaire, P.; Eriksson, S.; Stålberg, M.; Leijon, M.; Bernhoff, H. Design of a 12 kW vertical axis wind turbine equipped with a direct driven PM synchronous generator. In Proceedings of the EWEC 2006-European wind Energy Conference & Exhibition, Athens, Greece, 27 February–2 March 2006.
11. Deglaire, P.; Eriksson, S.; Kjellin, J.; Bernhoff, H. Experimental results from a 12 kW vertical axis wind turbine with a direct driven PM synchronous generator. In Proceedings of the EWEC 2007-European Wind Energy Conference & Exhibition, Milan, Italy, 7–10 May 2007.
12. Kjellin, J.; Eriksson, S.; Deglaire, P.; Bülow, F.; Bernhoff, H. Progress of control system and measurement techniques for a 12 kW vertical axis wind turbine. In Proceedings of the EWEC 2008-European Wind Energy Conference & Exhibition, Brüssels, Belgium, 31 March–3 April 2008.
13. Eriksson, S.; Solum, A.; Leijon, M.; Bernhoff, H. Simulations and experiments on a 12 kW direct driven PM synchronous generator for wind power. *Renew. Energy* **2008**, *33*, 674–681.
14. Kjellin, J.; Bülow, F.; Eriksson, S.; Deglaire, P. Power coefficient measurement on a 12 kW straight bladed vertical axis wind turbine. *Renew. Energy* **2011**, *36*, 3050–3053.
15. Sheldahl, R.E.; Klimas, P.C. Aerodynamic characteristics of seven symmetrical airfoil sections through 180-degree angle of attack for use in aerodynamic analysis of vertical axis wind turbines. In *Technical Report SAND80-2114*; Sandia National Laboratories: Albuquerque, NM, USA, 1981.

16. Halldin, S.; Bergström, H.; Gustafsson, D.; Dahlgren, L.; Hjelm, P.; Lundin, L.C.; Mellander, P.E.; Nord, T.; Jansson, P.E.; Seibert, J.; *et al*. Continuous long-term measurements of soil-plant-atmosphere variables at an agricultural site. *Agric. For. Meteorol.* **1999**, *98–99*, 75–102.
17. Power performance measurements of electricity producing wind turbines. In *Technical Report IEC 61400-12-1:2005(E)*; International Electrotechnical Commission: Geneva, Switzerland, 2005.
18. Bohn, C.; Atherton, D.A. Analysis package comparing PID anti-windup strategies. *IEEE Control Syst. Mag.* **1995**, *15*, 34–40.